



CrossMark
click for updates

Cite this: *RSC Adv.*, 2016, 6, 10272

Hierarchically porous NiO–Al₂O₃ nanocomposite with enhanced Congo red adsorption in water

Chunsheng Lei,^{ab} Xiaofeng Zhu,^b Yao Le,^a Bicheng Zhu,^a Jiaguo Yu^{*ad} and Wingkei Ho^{*c}

Congo red (CR) has been widely used in the textile industry. However, the discharge of wastewater containing CR is a subject of great concern with regard to environmental protection. Herein, NiO, Al₂O₃, and NiO–Al₂O₃ nanocomposite adsorbents with hierarchical porous structures were prepared by a simple solvothermal method. Adsorption removal of CR dye from aqueous solutions was investigated using the prepared samples as adsorbent, which had hierarchical porous structures composed of mesopores (2–50 nm) and macropores (>50 nm). The equilibrium adsorption data of CR on the NiO–Al₂O₃ samples were well fitted by the Langmuir model and yielded a maximum adsorption amount of 357 mg g⁻¹, which was higher than that of NiO and Al₂O₃ samples. The high adsorption of the NiO–Al₂O₃ nanocomposite sample was caused by the synergic effect of its hierarchical porous structures, high specific surface area, and positive surface charge at pH 7. Adsorption kinetic data could be well fitted by the pseudo-second-order kinetic equation, suggesting that pseudo-second-order kinetics could well represent the adsorption kinetics of the NiO–Al₂O₃ samples. The calculated activation energy needed by NiO–Al₂O₃ samples to adsorb CR indicated that the adsorption of CR molecules on NiO–Al₂O₃ sample was facilitated by physical adsorption process.

Received 8th November 2015
Accepted 18th January 2016

DOI: 10.1039/c5ra23545f

www.rsc.org/advances

1. Introduction

In recent years, various dyes have been detected in the effluents of some industries, including textiles, leather, paper, dyes, and plastics. Every year, more than 100 000 known commercial dyes are produced, and about 100 tons per year are discharged into rivers and lakes.^{1–5} Therefore, large amounts of dye wastewater have caused serious environmental pollution problems.^{6–8} Congo red (CR) is one of the most typical synthetic dyes and has been widely used in the textile industry. CR is a sodium salt of benzidinediazobis-1-naphthylamine-4-sulfonic acid, and the molecular structure of CR is shown in Fig. 1. CR is considered to be hazardous and toxic to many organisms. Specifically, the degraded by-products of CR usually contain toxic aromatic amine compounds, which are carcinogenic and harmful to the skin, eyes, blood, and reproductive cells of the human body. Despite being banned in many countries because of its health hazards and adverse environmental effects, CR is still used in some countries.^{9–12} Thus, treatment of dye wastewater discharge to

reduce the CR concentration below the permissible limit has become a subject of priority, thereby protecting the environment and preserving habitats. Various methods have been developed and used for the removal of CR from dye wastewater, including physical adsorption, coagulation/flocculation, advanced oxidation processes, membrane filtration, photocatalysis, ozonation, and biological treatment.^{13–16} Among these treatment methods, adsorption has been recognized as one of the most important methods owing to the advantages of high efficiency, low cost, simple operation, and easy recovery. Moreover, adsorption does not produce harmful by-products.^{17–21}

In recent years, many adsorbents for the removal of pollutants from wastewater have been intensively studied, including activated carbons from cheap carbon sources,^{22–24} fly ash,^{25–27} and clay minerals.^{28–30} Usually, adsorbents with large surface areas and hierarchical porous structures are required.^{31,32} In addition, wastewater with anionic dyes such as CR often

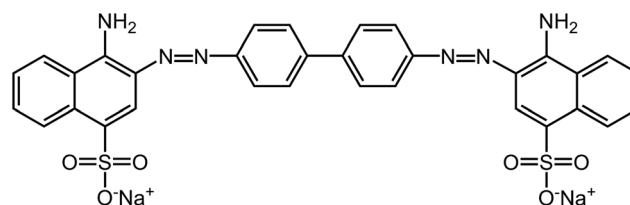


Fig. 1 Molecular structure of Congo red molecule.

^aState Key Laboratory of Advanced Technology for Material Synthesis and Processing, Wuhan University of Technology, Luoshi Road 122#, Wuhan 430070, PR China

^bCollege of Environmental and Security Engineering, Changzhou University, Gehu Road 1#, Changzhou 213164, PR China

^cDepartment of Science and Environmental Studies and Centre for Education in Environmental Sustainability, The Hong Kong Institute of Education, Tai Po, N.T., Hong Kong, P.R. China. E-mail: keithho@ied.edu.hk

^dFaculty of Science, King Abdulaziz University, Jeddah 21589, Saudi Arabia

contains other cationic and neutral dye pollutants. The presence of these other pollutants in wastewater sometimes reduces the efficiency of adsorbents for anionic dye removal.³³ Therefore, the selectivity of adsorbents needs to be identified for efficient wastewater treatment.

NiO is an important functional material widely used in catalysis, battery, electrochromic films, and fuel cell electrodes. Al₂O₃ has also been widely used as catalyst, catalytic support, adsorbent, and wear-resistant coating. Compared with the individual performances of NiO and Al₂O₃, NiO–Al₂O₃ nanocomposites are usually more efficient catalysts and have been used in industrial processes, including hydrogenation, dehydrogenation, petroleum refining, methanation, CO₂ reduction, and fuel cell operations.^{34–36} Therefore, many studies have reported the synthesis and application of NiO–Al₂O₃ nanostructures.^{37–44} For example, Crisan *et al.* reported the preparation of NiO/Al₂O₃ catalysts using sol–gel method,³⁵ whereas Zhang *et al.* prepared NiO/γ-Al₂O₃ catalysts by combining sol–gel and impregnation methods.³⁷ However, the preparation of hierarchically porous NiO–Al₂O₃ nanocomposites and their application as adsorbent in water treatment have been rarely studied. Herein, we provide the first report on the synthesis of hierarchical porous NiO–Al₂O₃ nanocomposites as adsorbents and their application in the removal of CR from water. This study will provide new insights into the design and fabrication of high-performance adsorption materials to perform Congo red adsorption from waste water.

2. Experimental

2.1. Material synthesis

All reagents such as Al(NO₃)₃·9H₂O, Ni(NO₃)₂·6H₂O, urea, and ethanol were of analytical grade (purchased from Shanghai Chemical Industrial Company) and were used without further purification. Distilled water was used for all synthesis and treatment processes.

NiO–Al₂O₃ nanocomposites were synthesized by a simple solvothermal method. In a typical preparation, 0.009 mol Ni(NO₃)₂·6H₂O and 0.003 mol Al(NO₃)₃·9H₂O were dissolved in 80 mL ethanol solution containing 0.2 mol urea. After stirring at room temperature for 60 min, the mixed solution was transferred to a 100 mL Teflon-lined stainless steel autoclave, which was heated to 140 °C and kept at the same temperature for 14 h. Then, the autoclave was cooled to 25 °C. The produced precipitate was alternately washed five times with water and ethanol and dried at 80 °C for 6 h. The air-dried precipitate was heated to 500 °C at a rate of 2 °C min^{−1} and kept at 500 °C for 2 h. The calcined sample was labeled NA. For comparison, the same experimental procedure was repeated for the preparation of single NiO and Al₂O₃, which were labeled N and A, respectively (Table 1).

2.2. Characterization

The X-ray diffraction (XRD) patterns were obtained using an X-ray diffractometer (type HZG41B-PC) with Cu Kα radiation (λ = 1.5406 Å), which were used to investigate the phase structure

Table 1 Preparation parameters of the NA, N, and A samples

Samples	Composition	Ni(NO ₃) ₂ (mol)	Al(NO ₃) ₃ (mol)	[Ni ²⁺]: [Al ³⁺] molar ratio
NA	NiO–Al ₂ O ₃	0.009	0.003	3 : 1
N	NiO	0.009	0.000	9 : 0
A	Al ₂ O ₃	0.000	0.003	0 : 3

and composition of the samples. Scanning electron microscopy (SEM) observation was performed using S-4800 field emission (Hitachi, Japan) and JSM-6510 (JEOL, Japan) scanning electron microscope. The elemental analysis of the prepared sample was conducted by an energy-dispersive X-ray spectrometer (EDS) attached to the FE-SEM. The Brunauer–Emmett–Teller (BET) specific surface area (S_{BET}) and pore structures of the powder samples were analyzed by nitrogen adsorption in a Micromeritics ASAP 2020 nitrogen adsorption apparatus (Micromeritics, USA). A desorption isotherm was used to determine the pore-size distribution through the Barrett–Joyner–Halenda method assuming a cylindrical pore model.⁴⁵ The nitrogen adsorption volume at a relative pressure (P/P_0) of 0.994 was used to determine the pore volume and average pore size. The Fourier transform infrared (FTIR) spectra of the samples before and after adsorption were recorded on a Shimadzu IR Affinity-1 spectrometer using KBr pellets as support in the wavenumber range of 4000–500 cm^{−1}. The isoelectric points (IEP) of the samples were measured on Malvern Zetasizer Nano-ZS90 (Malvern, UK).

2.3. Adsorption equilibrium and kinetic studies

Adsorption isotherm studies were conducted by adding 10 mg of the prepared NA, N, or A samples to a series of 250 mL conical flasks with 50 mL CR solutions at various concentrations (10–100 mg L^{−1}) at pH *ca.* 7. The conical flasks were sealed and stirred in a thermostatic shaker at 150 rpm for 12 h at 30 °C. After adsorption, the conical flasks were taken from the shaker and the final CR concentration in the supernatant solution was measured according to the maximum adsorption peak of CR (497 nm) using a UV/Vis spectrophotometer (Shimadzu UV/Vis 1240 spectrophotometer, Japan). The amount of CR adsorbed on the adsorbent sample at equilibrium q_e (mg g^{−1}) was calculated using the following equation:

$$q_e = \frac{(C_0 - C_e)V}{W} \quad (1)$$

where C_0 and C_e (mg L^{−1}) represent the beginning and equilibrium concentrations of CR in aqueous solution, respectively; and W and V are the mass (g) of the adsorbent used and the volume (L) of the solution, respectively.

Adsorption kinetic experiments were performed to investigate the effect of adsorption time on adsorption rate. The initial concentration of CR was fixed at 50 mg L^{−1}. Then, the aqueous samples were taken at pre-set time intervals and the CR concentrations were measured as previously described. The amount of adsorption at t time (q_t [mg g^{−1}]) was calculated using the following equation:

$$q_t = \frac{(C_0 - C_t)V}{W} \quad (2)$$

where C_0 and C_t (mg L^{-1}) represent the beginning and t time concentrations of CR in the solution, respectively; W is the mass (g) of adsorbent samples; and V is the volume (L) of the CR solution.

3. Results and discussion

3.1. XRD

The phase structures of the prepared samples were investigated by XRD. Fig. 2 presents the comparison of XRD patterns from the NA, N, and A samples. The XRD pattern of the NA sample shows NiO peaks (JCPDS data card no. 65-2901) and NiAl_2O_4 peaks (JCPDS data card no. 10-0339), indicating that the NA sample contains NiO and NiAl_2O_4 in two phases. The XRD patterns of the N and A samples show that they mainly consist of NiO and Al_2O_3 (JCPDS data card no. 50-0741), respectively.

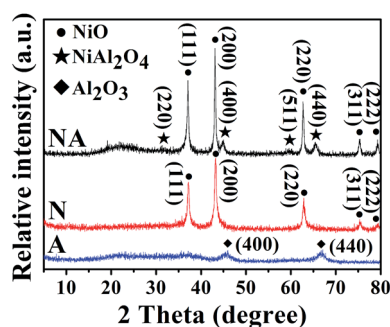


Fig. 2 XRD patterns of the NA, N, and A samples.

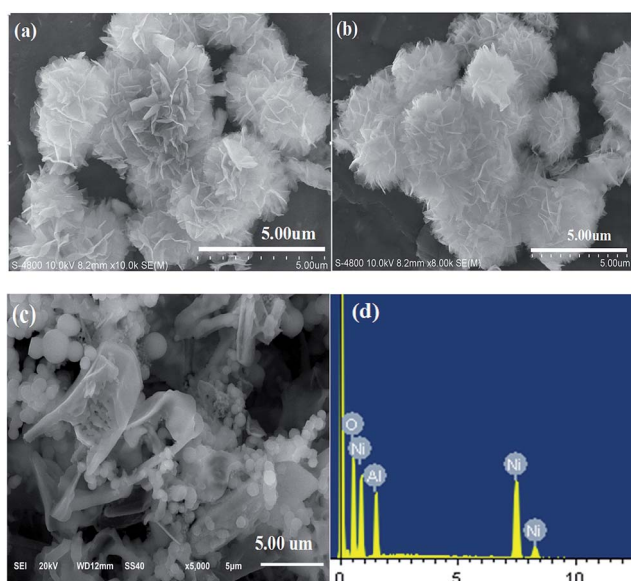


Fig. 3 SEM images of the NA (a), N (b), and A (c) samples; and the EDS spectrum of the NA sample (d).

3.2. SEM-EDS

The morphology and surface microstructure of the samples were observed by FE-SEM (Fig. 3). The SEM image of the NA sample (Fig. 3a) indicates that the $\text{NiO-Al}_2\text{O}_3$ nanocomposites have highly porous textures composed of ca. $5.0 \mu\text{m}$ sized microspheres assembled from building blocks of 2D nanosheets. The morphology of the N sample is highly similar to that of NA, which is also composed of 2D nanosheets (shown in Fig. 3b) and also has an obviously layered structure. The SEM image of the A sample is different from that of the NA and N samples, containing irregularly thick plates and uniform spherical particles and exhibiting an irregular and ill-defined morphology (Fig. 3c). The EDS analysis of the NA sample (Fig. 3d) indicates the presence of Ni, Al, and O elements.

3.3. Nitrogen adsorption

The nitrogen adsorption–desorption isotherms and the corresponding pore-size distribution curves of the prepared NA, N, and A samples are presented in Fig. 4a and b. The three samples are type IV isotherms according to the Brunauer–Deming–Deming–Teller (BDDT) classification.⁴⁵ The hysteresis loops of the NA and N samples are relatively smaller than those of the A sample because of their better crystallization (Fig. 2) and lower pore volume. The hysteresis loops of the NA and N samples are of typical H3 type at high relative pressure (approaching 1), indicating the presence of slit-shaped mesopores and macropores from the aggregation of 2D nanosheets within the microsphere (Fig. 3a and b). However, the A sample has higher nitrogen

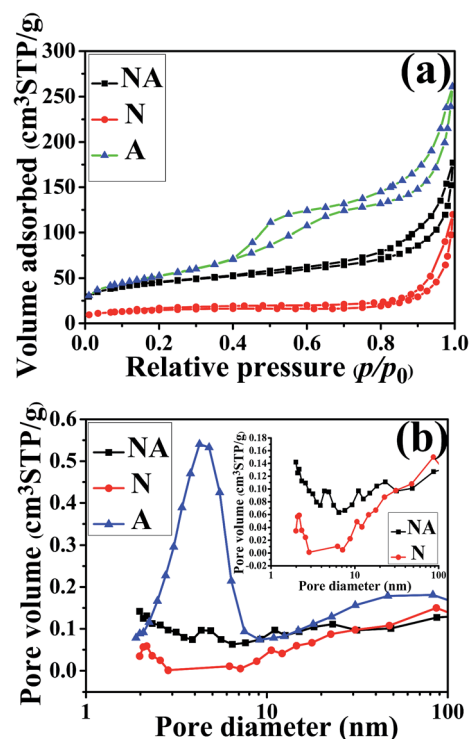


Fig. 4 Nitrogen adsorption–desorption isotherms (a) and corresponding pore-size distribution curves (b) of the NA, N, and A samples.

Table 2 Specific surface areas and pore parameters of the NA, N, and A samples^a

Samples	Composition	APS (nm)	PV (cm ³ g ⁻¹)	S _{BET} (m ² g ⁻¹)
NA	NiO–Al ₂ O ₃	4.7	0.18	157
N	NiO	7.6	0.09	52
A	Al ₂ O ₃	6.5	0.31	188

^a APS: average pore size; PV: pore volume.

adsorption–desorption isotherms compared with the NA and N samples, suggesting its larger specific surface area owing to its weak crystallization (Fig. 2). Further observation indicates that the A sample has two evident hysteresis loops. At a low relative pressure range of 0.4–0.7, the hysteresis loop is type H2, which indicates that the A sample contains ink-bottle pores (with narrow necks and wide bodies) caused by the aggregation of nanoparticles. Meanwhile, at a high relative pressure range of 0.7–1.0, the loop is type H3, which is related to the plate-like particles that form slit-shaped pores. The pore size distribution curves of the three samples (Fig. 4b) present a wide pore range from 2 nm to more than 100 nm, which implies that the prepared NA, N, and A samples contain hierarchically porous structures.^{46–49} The average pore size, pore volume, and BET surface areas of the NA, N, and A samples are listed in Table 2. These results indicate that because of its weaker crystallization, thus small crystallite size, the A sample has larger specific surface area and pore volume than the NA and N samples have.⁴⁷

3.4. FTIR spectra

To identify the functional groups of CR and determine the interaction between the prepared samples and CR during the adsorption process, FTIR spectra of the NA sample before and after CR adsorption are shown in Fig. 5a and b, respectively. The broad absorption vibration bands at 3449 and 1376 cm⁻¹ are attributed to the stretching vibration of the –OH group from water molecules (physical adsorption of molecular water),⁴⁴ whereas the band at 2930 cm⁻¹ is attributed to C–H stretching vibration.⁵⁰ The band at 2370 cm⁻¹ is caused by the stretching vibration of CO₂ from CO₂ adsorption on the surface of the

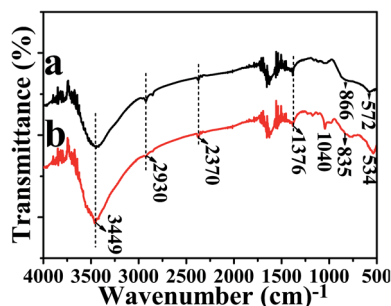


Fig. 5 FTIR spectra of the NA sample before (a) and after (b) adsorption of CR.

sample. The bands at 866 and 835 cm⁻¹ are from the vibrational modes of the surface Al–O bond,^{50,51} whereas the bands at 572 and 534 cm⁻¹ are due to Ni–O stretching vibration.⁵² The characteristic band observed at 1040 cm⁻¹ belongs to the symmetric and asymmetric stretching vibrations of S=O in CR molecules.⁵³ FTIR results indicate that CR molecules indeed adsorb on the NA sample surface.

3.5. Adsorption kinetics

Adsorption kinetics is crucial in adsorption investigation because it can predict the adsorption removal rate of a pollutant from aqueous solutions. It can also enhance the understanding on adsorption mechanism. Because of the novel hierarchical porous structure and large specific surface area, the NA sample should have good adsorption affinity toward dye molecules in water. Thus, the CR dye adsorption activity of the NA sample in water was studied using batch adsorption kinetic experiments. Fig. 6 presents the comparison of CR adsorption kinetics on the NA, N, and A samples, which were performed by batch adsorption tests at a fixed initial CR concentration (50 mg L⁻¹) at 30 °C. During the first 25 min, the NA, N, and A samples all presented high adsorption rates; and after 150 min, adsorption equilibrium was achieved. Although the same experimental conditions were used for all three samples, the differences in adsorption rate and capacity were clearly observed. The NA sample had the largest adsorption capacity, followed by N sample, and finally, the A sample. Notably, the A sample had the largest BET specific surface area (188 m² g⁻¹), but it possessed the lowest adsorption capacity of about 120 mg g⁻¹, indicating that the specific surface area is not the only factor that influences adsorption. On the contrary, other factors, such as surface charge of the sample, probably have greater influence on adsorption than specific surface area.

To investigate the surface charges of the NA, N, and A samples in water, their zeta potentials were analyzed by Malvern Zetasizer Nano ZS90. The variations in zeta potentials of NA, N, and A samples along with the pH value of the suspensions are shown in Fig. 7. For the suspension with the initial pH (at *ca.* 7), the zeta potentials of the NA, N, and A samples were 10.0, 16.9, and 2.0 mV, respectively. The zeta potentials gradually

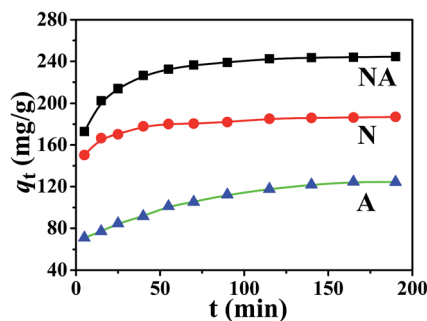


Fig. 6 Changes in adsorption capacities with adsorption times for CR molecules adsorbed on the NA, N, and A samples ($T = 30$ °C, adsorbent dose = 200 mg L⁻¹, CR concentration = 50 mg L⁻¹, and pH = 7).

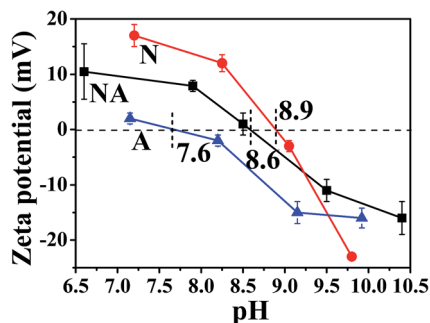


Fig. 7 Variation in zeta potentials with pH value of the suspensions of the NA, N, and A samples.

decreased as pH value increased. In addition, the IEP of NA, N, and A samples were 8.6, 8.9, and 7.6, respectively. Thus, the oxide particle surface was positively charged at pH values below the IEP but negatively charged above IEP. In addition, the zeta potential of A sample suspension was less positive than that of NA and N sample suspensions at a neutral environment. Expectedly, among the three samples, the A sample had the lowest adsorption capacity with negative CR molecules because of the extremely weak electrostatic interaction between the CR molecule and the A sample surface.⁵⁴

The above investigation and discussion indicate that the difference in the adsorption affinity of the samples toward pollutant molecules is mainly related to two key factors, namely, zeta potential and surface area of the samples. For example, the N sample has lower specific surface area ($52 \text{ m}^2 \text{ g}^{-1}$) but a more positive zeta potential (16.9 mV) and still exhibits higher adsorption capacity for CR molecules than the A sample. This illustration indicates that, compared with specific surface area, surface charge has a stronger influence on the affinity and adsorption of the sample surface toward pollutant molecules. Thus, it is expected that among the three samples, the NA sample exhibited the highest adsorption capacity toward CR molecules because of its relatively large specific surface area and positive zeta potential. The hierarchically porous structures of the NA sample, which facilitated the transport and diffusion of pollutant molecules in the adsorbent, also enhanced its adsorption activity toward CR molecules.

Further investigation indicates that the adsorption kinetic data of the NA, N, and A samples can be well fitted by a pseudo-second-order kinetic equation as follows:⁵⁵

$$\frac{t}{q_t} = \frac{1}{kq_e^2} + \frac{t}{q_e} \quad (3)$$

where q_t and q_e (mg g^{-1}) represent the adsorption amount of CR at time t (min) and equilibrium, respectively; and k ($\text{g mg}^{-1} \text{ min}^{-1}$) is the pseudo-second-order rate constant. The linear relationship of t/q_t versus t is presented in Fig. 8, and the calculated kinetic parameters are listed in Table 3. The obtained R^2 values were greater than 0.995 for samples NA, N, and A, and the normalized standard deviation S.D. (%) values were lower than 1.82 for all the three samples. For statistical analysis, the

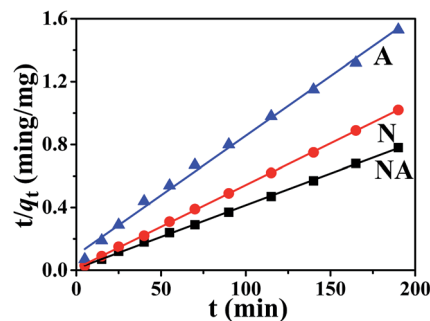


Fig. 8 Pseudo-second-order kinetics of the NA, N, and A samples for CR adsorption ($T = 30 \text{ }^\circ\text{C}$, adsorbent dose = 200 mg L^{-1} , CR concentration = 50 mg L^{-1} , and $\text{pH} = 7$).

Table 3 Parameters of the pseudo-second-order adsorption kinetics of NA, N, and A samples

Samples	C_0 (mg L^{-1})	$q_{e,\text{exp}}$ (mg g^{-1})	Pseudo-second-order model			
			$q_{e,\text{cal}}$ (mg g^{-1})	k ($\times 10^{-4} \text{ g mg}^{-1} \text{ min}^{-1}$)	R^2	S.D. (%)
NA	50	244	250	5.9	0.999	0.71
N	50	187	189	2.4	0.999	0.30
A	50	124	132	1.6	0.995	1.82

number of the samples studied was 5. Both equilibrium adsorption amount and k value follow the order $\text{NA} > \text{N} > \text{A}$.

Adsorption kinetics data of the NA sample were also tested at different adsorption temperatures (25, 35, and $45 \text{ }^\circ\text{C}$) to calculate the activation energy (E_a) of adsorption. The E_a was estimated using the Arrhenius equation.⁵⁶

$$\ln k_2 = \ln A - \frac{E_a}{RT} \quad (4)$$

where E_a and k_2 represent the Arrhenius activation energy (kJ mol^{-1}) and the pseudo-second-order rate constant, respectively. A , R , and T represent the Arrhenius factor, gas constant ($8.314 \text{ J mol}^{-1} \text{ K}^{-1}$), and the absolute temperature, respectively. When $\ln k_2$ versus $1/T$ was plotted, a straight line with the slope $-E_a/R$ was obtained (not shown here). The level of E_a can be used to determine the type of adsorption, that is, chemical or physical adsorption. Physical adsorption often has E_a in the range of $0\text{--}40 \text{ kJ mol}^{-1}$, whereas chemical adsorption has higher E_a at $40\text{--}800 \text{ kJ mol}^{-1}$. The above calculated E_a is 19.8 kJ mol^{-1} , indicating that the CR molecules were physically adsorbed on the surface of the NA sample.^{4,56,57}

3.6. Adsorption isotherms

The adsorption isotherms of CR on the NA, N, and A samples are presented in Fig. 9. These adsorption isotherms were fitted using the Langmuir and Freundlich models. The Langmuir model assumes that no interaction occurs among adsorbate molecules, and that the adsorption is a monolayer.

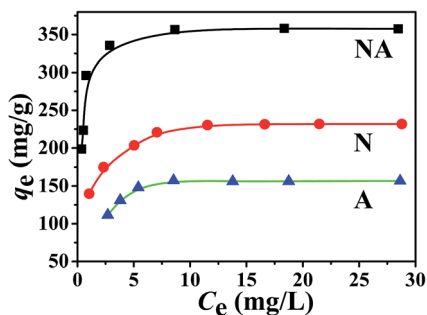


Fig. 9 Adsorption isotherms of the NA, N, and A samples for CR ($T = 30\text{ }^{\circ}\text{C}$, adsorbent dose = 200 mg L^{-1} , CR concentration = $10\text{--}100\text{ mg L}^{-1}$, and $\text{pH} = 7$).

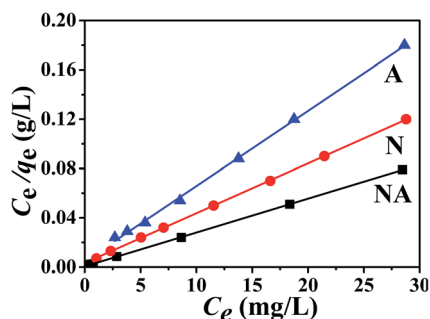


Fig. 10 Langmuir isotherms of the NA, N, and A samples for CR adsorption at $30\text{ }^{\circ}\text{C}$.

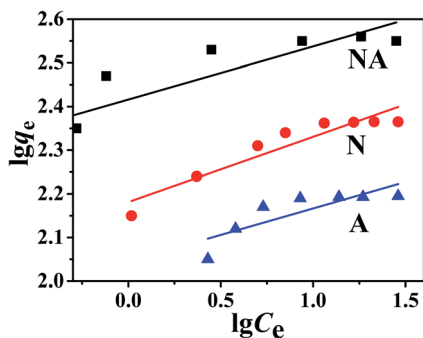


Fig. 11 Freundlich isotherms of the NA, N, and A samples for CR adsorption at $30\text{ }^{\circ}\text{C}$.

Additionally, once a site is occupied by an adsorbate molecule, no further adsorption can occur. However, the Freundlich adsorption model assumes that adsorption occurs on

heterogeneous surfaces. The linear equations of Langmuir and Freundlich isotherm are expressed as follows:^{58–62}

$$\frac{C_e}{q_e} = \frac{C_e}{q_{\max}} + \frac{1}{K_L q_{\max}} \quad (5)$$

$$\ln q_e = \ln K_F + \frac{1}{n} \ln C_e \quad (6)$$

where C_e is the equilibrium concentration of CR in the solution (mg L^{-1}), q_e is the equilibrium capacity of CR on the adsorbent (mg g^{-1}), and q_{\max} is the maximum adsorption capacity of the adsorbent corresponding to a complete monolayer coverage on the surface (mg g^{-1}). K_L is the Langmuir adsorption constant (L mg^{-1}) associated with the free energy of adsorption, which can be obtained from the intercepts and slopes of the linear plots of C_e/q_e versus C_e (Fig. 10). K_F is the Freundlich constant (mg g^{-1}) (L mg^{-1})^{1/n}, and $1/n$ is the heterogeneity factor. The fitted parameters and R^2 are listed in Table 2. Fig. 10 and 11 show that the experimental data can be better fitted by the Langmuir model, indicating the homogeneous nature of the sample surface and a monolayer adsorption of CR molecules on the outer surface of the adsorbent. According to the Langmuir fitting results (see Table 4), the maximum adsorption amount follows the order of $\text{NA} > \text{N} > \text{A}$. By combining the adsorption isotherms and CR kinetics of the three samples, the NiO and Al_2O_3 composite NA sample exhibited the best adsorption performance.

The adsorption selectivity of the NA sample was further investigated by selective adsorption of the mixed aqueous solution of CR and methylene blue (MB). The results (not shown here) indicated that the adsorption of CR was faster than that of MB at $\text{pH} 7$. This observation was caused by the negatively charged CR molecules preferentially adsorbed on the surface of the positively charged NA sample. By contrast, the NA sample had negative surface charge and exhibited better adsorption selectivity toward MB molecules at $\text{pH} 10$. The above adsorption selectivity experiments indicate that the selective adsorption of CR and MB on the NA sample surface can be easily tuned by simply changing the pH values of the CR and MB mixture. This also suggests the possibility of tuning the adsorption selectivity by simply modifying the surface charges of the samples in different pH . Moreover, the adsorption capacities of the prepared samples for CR are compared with the previously reported results and listed in Table 5, indicating that the hierarchical NiO- Al_2O_3 nanocomposite obtained in this work exhibited excellent adsorption performance for CR.

Table 4 Adsorption isotherm parameters of the NA, N, and A samples obtained by fitting in Langmuir and Freundlich isotherm equations

Samples	Langmuir isotherm model				Freundlich isotherm model		
	q_{\max} (mg g^{-1})	k_L ($\times 10^{-1}\text{ L mg}^{-1}$)	R^2	R_L	K_F (mg g^{-1}) (L mg^{-1}) ^{1/n}	n	R^2
NA	357	5.60	1.000	0.004	11.2	8.22	0.770
N	250	1.21	0.999	0.027	8.86	6.70	0.892
A	164	1.27	0.998	0.031	7.73	8.22	0.697

Table 5 The adsorption capacities of the prepared NiO–Al₂O₃ samples for CR compared with other reported results

Adsorbents	q_{\max} (mg g ⁻¹)	References
Hierarchical NiO–Al ₂ O ₃ nanocomposite	357	This work
Hierarchical NiO	250	This work
Al ₂ O ₃	164	This work
Hierarchical NiO nanosheets	152	60
Hierarchical Ni(OH) ₂ nanosheets	83	60
NiO–SiO ₂ hollow microspheres	204	63
Hollow hierarchical MnO ₂	60	64
Hierarchically structured γ -AlOOH	99	65
Porous ZrO ₂ hollow sphere	60	66
Maghemite nanoparticles	208	67
Mg–Al-layered double hydroxide	37	68
Activated carbon	300	69
Activated carbon	189	70

4. Conclusion

In summary, hierarchical porous NiO–Al₂O₃ nanocomposite particles were successfully prepared through a simple solvothermal method, which consisted of *ca.* 5.0 μm microspheres assembled from building blocks of 2D nanosheets. The prepared NiO–Al₂O₃ nanocomposite sample had stronger adsorption affinity toward CR in water than individual NiO or Al₂O₃ samples. This result was due to the prepared nanocomposite sample with relatively large specific surface area and positive zeta potential. Adsorption isotherms of the prepared NiO–Al₂O₃, NiO, and Al₂O₃ samples were fitted using Langmuir and Freundlich equations. The adsorption equilibrium data were well described by the Langmuir isotherm model, with maximum monolayer adsorption capacity of 357, 250, and 164 mg g⁻¹ for NiO–Al₂O₃, NiO, and Al₂O₃ samples, respectively. The adsorption kinetic data of the prepared samples were found to follow the pseudo-second-order kinetic equation. The calculated E_a for CR adsorption of the NiO–Al₂O₃ samples was 19.8 kJ mol⁻¹, indicating that the adsorption of CR molecules on the NiO–Al₂O₃ sample was facilitated by a physical adsorption. The FTIR results also indicate that the CR molecules can strongly adsorb on the surface of NiO–Al₂O₃ samples because of their strong electrostatic attraction. The prepared NiO–Al₂O₃ sample exhibited good adsorption selectivity to CR and MB molecules in water by simply changing the pH of the solution. The prepared NiO–Al₂O₃ composite sample is considered to be effective adsorbent for the removal of CR from water because of its unique hierarchical porous structure, positive surface charge, and large specific surface area.

Acknowledgements

This study was partially supported by the 973 Program (2013CB632402), NSFC (21433007, 51320105001 and 51272199), the Fundamental Research Funds for the Central Universities (2015-III-034), Self-determined and Innovative Research Funds of

SKLWUT (2015-ZD-1) and the Natural Science Foundation of Hubei Province of China (No. 2015CFA001) for Jiaguo Yu. This research was financially supported by the research grant of Early Career Scheme (ECS 809813) from the Research Grant Council, Hong Kong SAR Government, Dean's Research Fund-Early Career Researchers (04022), and Research Equipment Grant (REG-2) for Wingkei Ho. This work was supported by the National Natural Science Funds (Grant No. 51208068, BY2013118) for Chunsheng Lei.

References

- 1 T. K. Sen, S. Afroze and H. Ang, *Water, Air, Soil Pollut.*, 2011, **218**, 499.
- 2 M. T. Yagub, T. K. Sen and H. M. Ang, *Water, Air, Soil Pollut.*, 2012, **223**, 5267.
- 3 J. Hu, Z. Song, L. Chen, H. Yang, J. Li and R. Richards, *J. Chem. Eng. Data*, 2010, **55**, 3742.
- 4 M. Liu, J. Xu, B. Cheng, W. Ho and J. Yu, *Appl. Surf. Sci.*, 2015, **332**, 121.
- 5 A. Gottlieb, C. Shaw, A. Smith, A. Wheatley and S. Forsythe, *J. Biotechnol.*, 2003, **101**, 49.
- 6 M. S. Chiou, P. Y. Ho and H. Y. Li, *Dyes Pigm.*, 2004, **60**, 69.
- 7 W. Zhao, Y. Tang, J. Xi and J. Kong, *Appl. Surf. Sci.*, 2015, **326**, 276.
- 8 R. Wang, X. Cai and F. Shen, *Appl. Surf. Sci.*, 2014, **305**, 352.
- 9 V. Vimonses, S. M. Lei, B. Jin, C. W. K. Chow and C. Saint, *Chem. Eng. J.*, 2009, **148**, 354.
- 10 T. Hao, C. Yang, X. Rao, J. Wang, C. Niu and X. Su, *Appl. Surf. Sci.*, 2014, **292**, 174.
- 11 M. Akgül, *J. Hazard. Mater.*, 2014, **267**, 1.
- 12 S. Wei, X. Hu, H. Liu, Q. Wang and C. He, *J. Hazard. Mater.*, 2015, **294**, 168.
- 13 V. Gupta, *J. Environ. Manage.*, 2009, **90**, 2313.
- 14 V. A. Sakkas, M. A. Islam, C. Stalikas and T. A. Albanis, *J. Hazard. Mater.*, 2010, **175**, 33.
- 15 S. G. Kumar and K. S. R. Koteswara Rao, *Appl. Surf. Sci.*, 2015, **355**, 939.
- 16 J. Zhao, Y. Tan, K. Su, J. Zhao, C. Yang, L. Sang, H. Lu and J. Chen, *Appl. Surf. Sci.*, 2015, **337**, 111.
- 17 S. Mustafa, M. I. Zaman and S. Khan, *J. Colloid Interface Sci.*, 2006, **301**, 370.
- 18 M. T. Yagub, T. K. Sen, S. Afroze and H. M. Ang, *Adv. Colloid Interface Sci.*, 2014, **209**, 172.
- 19 L. Qi, J. Yu and M. Jaroniec, *Adsorption*, 2013, **19**, 557.
- 20 J. Yu, X. Li, Z. Xu and W. Xiao, *Environ. Sci. Technol.*, 2013, **47**, 9928.
- 21 K. Ouyang, C. Zhu, Y. Zhao, L. Wang, S. Xie and Q. Wang, *Appl. Surf. Sci.*, 2015, **355**, 5629.
- 22 M. K. Purkait, A. Maiti, S. DasGupta and S. De, *J. Hazard. Mater.*, 2007, **145**, 287.
- 23 Y. Gokce and Z. Aktas, *Appl. Surf. Sci.*, 2014, **313**, 352.
- 24 Y. Huang, S. Li, J. Chen, X. Zhang and Y. Chen, *Appl. Surf. Sci.*, 2014, **293**, 160.
- 25 B. H. Hameed, A. A. Ahmad and N. Aziz, *Chem. Eng. J.*, 2007, **133**, 195.
- 26 M. Visa, L. Isac and A. Duta, *Appl. Surf. Sci.*, 2015, **339**, 62.

- 27 E. Sočo and J. Kalemekiewicz, *J. Environ. Chem. Eng.*, 2013, **1**, 581.
- 28 B. Acemioğlu, *J. Colloid Interface Sci.*, 2004, **274**, 371.
- 29 A. Gurses, S. Karaca, Ç. Dogar, R. Bayrak, M. Açıklyıldız and M. Yalçın, *J. Colloid Interface Sci.*, 2004, **269**, 310.
- 30 M. Ji, X. Su, Y. Zhao, W. Qi, Y. Wang, G. Chen and Z. Zhang, *Appl. Surf. Sci.*, 2015, **344**, 128.
- 31 M. Khosravi and S. Azizian, *Colloids Surf., A*, 2015, **482**, 438.
- 32 P. Hu, D. Hou, H. Shi, C. Chen, Y. Huang and X. Hu, *Appl. Surf. Sci.*, 2014, **319**, 244.
- 33 S. Kagaya, H. Miyazaki, M. Ito, K. Tohda and T. Kanbara, *J. Hazard. Mater.*, 2010, **175**, 1113.
- 34 X. J. Zhang, J. X. Liu, Y. Jing and Y. C. Xie, *Appl. Catal., A*, 2003, **240**, 143.
- 35 M. Crisan, M. Zaharescu, V. D. Kumari, M. Subrahmanyam, D. Crisan, N. Dragan, M. Raileanu, M. Jitianu, A. Rusu, G. Sadanandam and J. K. Reddy, *Appl. Surf. Sci.*, 2011, **258**, 448.
- 36 H. Niazi, S. Yari, F. Golestani-Fard, M. Shahmiri, W. Wang, A. Alfantazi and R. Bayati, *Appl. Surf. Sci.*, 2015, **353**, 1242.
- 37 Y. Zhang, G. Xiong, S. Sheng and W. Yang, *Catal. Today*, 2000, **63**, 517.
- 38 L. X. Yang, Y. J. Zhu, H. Tong, Z. H. Liang and W. W. Wang, *Cryst. Growth Des.*, 2007, **7**, 2716.
- 39 X. F. Song and L. Gao, *J. Am. Ceram. Soc.*, 2008, **91**, 4105.
- 40 Z. Song, L. F. Chen, J. C. Hu and R. Richards, *Nanotechnology*, 2009, **20**, 275707.
- 41 W. Q. Cai, J. G. Yu and M. Jaroniec, *J. Mater. Chem.*, 2010, **20**, 4587.
- 42 N. F. M. Salleh, A. A. Jalil, S. Triwahyono, J. Efendi, R. R. Mukti and B. H. Hameed, *Appl. Surf. Sci.*, 2015, **349**, 485.
- 43 Y. C. Song, J. Wang, Z. S. Li, D. H. Guan, T. Mann, Q. Liu, M. L. Zhang and L. H. Liu, *Microporous Mesoporous Mater.*, 2012, **148**, 159.
- 44 W. L. Yang, Z. Gao, J. Wang, J. Ma, M. L. Zhang and L. H. Liu, *ACS Appl. Mater. Interfaces*, 2013, **5**, 5443.
- 45 K. S. W. Sing, D. H. Everett, R. A. W. Haul, L. Moscou, R. A. Pierotti, J. Rouquerol and T. Siemieniewska, *Pure Appl. Chem.*, 1985, **57**, 603.
- 46 X. X. Yu, J. G. Yu, B. Cheng and M. Jaroniec, *J. Phys. Chem. C*, 2009, **113**, 17527.
- 47 L. Qi, B. Cheng, W. Ho, G. Liu and J. Yu, *ChemNanoMat*, 2015, **1**, 58.
- 48 J. Jin, J. Yu, D. Guo, C. Cui and W. Ho, *Small*, 2015, **11**, 5262.
- 49 P. Lv, H. Zhao, Z. Zeng, C. Gao, X. Liu and T. Zhang, *Appl. Surf. Sci.*, 2015, **329**, 301.
- 50 S. K. Yadav and P. Jeevanadam, *J. Alloys Compd.*, 2014, **610**, 567.
- 51 M. Crisan, M. Zaharescu, V. D. Kumari, M. Subrahmanyam, D. Crisan, N. Dragan, M. Raileanu, M. Jitianu, A. Rusu, G. Sadanandam and J. K. Reddy, *Appl. Surf. Sci.*, 2011, **258**, 448.
- 52 P. Jeevanadam, Y. Kolytynin and A. Gedanken, *Mater. Sci. Eng., B*, 2002, **90**, 125.
- 53 H. X. Guo, J. H. Chen, W. Weng, Z. S. Zheng and D. F. Wang, *J. Ind. Eng. Chem.*, 2014, **5**, 3081.
- 54 B. Zhu, P. Xia, W. Ho and J. Yu, *Appl. Surf. Sci.*, 2015, **344**, 188.
- 55 I. A. W. Tan, A. L. Ahmad and B. H. Hameed, *J. Hazard. Mater.*, 2009, **164**, 473.
- 56 J. Zhou, C. Tang, B. Cheng, J. Yu and M. Jaroniec, *ACS Appl. Mater. Interfaces*, 2012, **4**, 2174.
- 57 J. J. Fan, W. Q. Cai and J. G. Yu, *Chem.-Asian J.*, 2011, **6**, 2481.
- 58 I. Langmuir, *J. Am. Chem. Soc.*, 1918, **40**, 1361.
- 59 H. M. F. Freundlich, *J. Phys. Chem.*, 1906, **57**, 385.
- 60 B. Cheng, L. Yao, W. Q. Cai and J. G. Yu, *J. Hazard. Mater.*, 2011, **185**, 889.
- 61 R. X. Chen, J. G. Yu and W. Xiao, *J. Mater. Chem. A*, 2013, **1**, 11682.
- 62 B. H. Hameed, A. A. Ahmad and N. Aziz, *Chem. Eng. J.*, 2007, **133**, 195.
- 63 C. S. Lei, X. F. Zhu, B. C. Zhu, J. G. Yu and W. K. Ho, *J. Colloid Interface Sci.*, 2016, **466**, 238.
- 64 J. B. Fei, Y. Cui, X. H. Yan, W. Qi, Y. Yang, K. W. Wang, Q. He and J. B. Li, *Adv. Mater.*, 2008, **20**, 452.
- 65 F. Meng, G. Rong, X. Zhang and W. Huang, *Mater. Lett.*, 2014, **129**, 114.
- 66 C. Wang, Y. Le and B. Cheng, *Ceram. Int.*, 2014, **40**, 10847.
- 67 A. Afkhami and R. Moosavi, *J. Hazard. Mater.*, 2010, **174**, 398.
- 68 R. Shan, L. Yan, Y. Yang, K. Yang, S. Yu, H. Yu, B. Zhu and B. Du, *J. Ind. Eng. Chem.*, 2015, **21**, 561.
- 69 M. K. Purkait, A. Maiti, S. DasGupta and S. De, *J. Hazard. Mater.*, 2007, **145**, 287.
- 70 E. Lorenc-Grabowska and G. Gryglewicz, *Dyes Pigm.*, 2007, **74**, 34.